# Artificial surfaces simulating complex terrain types for evaluating grid-based flow direction algorithms

Cheng-Zhi Qin [a] , Li-Li Bao [a] , A-Xing Zhu [a b] , Xue-Mei Hu [a] & Biao Qin [a]

[a] State Key Laboratory of Resources and Environmental Information System, Institute of Geographic Sciences and Natural Resources Research, Chinese Academy of Sciences, Beijing, PR China

[b] Department of Geography, University of Wisconsin-Madison, Madison, WI, USA
Version of record first published: 14 Nov 2012.

PLEASE SCROLL DOWN FOR ARTICLE

demand, or costs or damages whatsoever or howsoever caused arising directly or indirectly in connection with or arising out of the use of this material.

# Artificial surfaces simulating complex terrain types for evaluating grid-based flow direction algorithms

Cheng-Zhi Qin[a]*, Li-Li Bao[a], A-Xing Zhu[a,b], Xue-Mei Hu[a] and Biao Qin[a]

*[a]State Key Laboratory of Resources and Environmental Information System, Institute of Geographic Sciences and Natural Resources Research, Chinese Academy of Sciences, Beijing, PR China;
[b]Department of Geography, University of Wisconsin-Madison, Madison, WI, USA*

This article presents a set of artificial surfaces simulating complex terrain types for evaluating the performances of grid-based flow direction algorithms. The proposed artificial surfaces were developed based on sine and cosine functions and thus can simulate four complex terrain types: a convex-centred slope, concave-centred slope, saddle-centred slope and straight-ridge slope; such features are typical and widespread in real landscapes. We analytically solved the theoretical values of specific catchment area (SCA) for the proposed artificial surfaces. Compared with existing artificial surfaces for evaluating flow direction algorithms, the proposed artificial surfaces provide a better representation of common terrain types in the real world. To analyse the feasibility of the proposed artificial surfaces, two sets of artificial digital elevation models (DEMs) were created by sampling the proposed artificial surfaces with different reliefs at a series of resolutions (i.e. 1, 5, 10 and 20 m). Four representative flow direction algorithms were applied to these artificial DEMs: D8, D-inf, FD8 and MFD-md. The root mean square error, mean error and standard deviation in the computed SCA from flow direction algorithm show that MFD-md generally yielded lower error under simulated terrain conditions than D8, D-inf and FD8. The cumulative frequency distributions of errors from the tested flow direction algorithms with the proposed artificial DEMs can effectively reflect the inherent characteristics of each algorithm. MFD-md performed more similarly to FD8 in low-relief terrains and more similarly to D-inf in high-relief terrains. The map of errors from each tested algorithm is available for a spatially explicit evaluation of the occurrence of errors. Over most of the area, the D-inf algorithm underestimated the SCA when FD8 overestimated the SCA.

**Keywords:** artificial surface; error assessment; specific catchment area; flow direction algorithm; gridded digital elevation models

## 1. Introduction

Specific catchment area (SCA, or specific contributing area), which is defined as the upslope contributing area per unit contour length, is one of the most important topographic attributes (Moore *et al*. 1991, Hengl and Reuter 2009). SCA is widely used not only as a basis for many secondary topographic attributes, such as topographic wetness index and stream power index, but also in many hydrological, pedagogical and geomorphological applications (Wilson and Gallant 2000). In real applications, computation of SCA is

---

*Corresponding author. Email: qincz@lreis.ac.cn

generally dependent on a flow direction algorithm designed to be compatible with gridded digital elevation models (DEMs) (Li *et al*. 2005).

To date, many grid-based flow direction algorithms have been designed to calculate SCA (e.g. O'Callaghan and Mark 1984, Freeman 1991, Quinn *et al*. 1991, Costa-Cabral and Burges 1994, Quinn *et al*. 1995, Tarboton 1997, Qin *et al*. 2007, Zhou *et al*. 2011). Recently, Wilson *et al*. (2008) provided a thorough review of the current flow direction algorithms. The key difference between these algorithms is if the flow from a cell can be drained into more than one downslope neighbouring cell and if so, how to partition the flow among the downslope neighbouring cells. Different flow direction algorithms might produce very different SCA results (Wolock and McCabe 1995, Wilson *et al*. 2008); therefore, an error assessment of flow direction algorithms is vital (Zhou and Liu 2002).

Real DEMs are often applied to the assessment of flow direction algorithms (Wolock and McCabe 1995, Wilson and Gallant 2000). However, real DEMs are discrete representations of actual continuous topographic surface and contain errors that are hardly known spatially. Thus, the assessment of flow direction algorithms using real DEMs can only be relative or comparative. It is affected not only by the flow direction algorithms involved but also by the real data containing errors (Zhou and Liu 2002). Furthermore, the 'true' SCA of actual topography is hardly to be calculated analytically. Gallant and Hutchinson (2011) recently proposed the first method to calculate the 'true' SCA on real DEMs by solving a differential equation, which defines the rate of change of SCA along flow path as a function of SCA and plan curvature on the path. However, a numerical solution required is by converting the DEM to a mathematical surface with continuous first derivatives and piecewise continuous second derivatives (Gallant and Hutchinson 2011). As a result, the computed SCA for the same area may vary due to the choice of DEMs as well as the interpolation methods.

Artificial surfaces have been developed to evaluate the performances of flow direction algorithms (Zhou and Liu 2002, Pan *et al*. 2004). Artificial surfaces are defined by mathematical functions; so the uncertainty associated with data errors can be avoided. Meanwhile, it is possible to analytically solve the theoretical SCA at any position on the artificial surface. Because the theoretical SCA keeps unchanged for a given artificial surface, the artificial surface can be sampled at different resolutions to create artificial DEMs with different grid sizes for a multiple-scale analysis (Qin *et al*. 2011). Thus, the performances of flow direction algorithms can be evaluated in a quantitative and data-independent way based on the difference between the theoretical SCA and computed SCA (Zhou and Liu 2002).

The simplest artificial surfaces ever proposed for evaluating flow direction algorithms are those with all contours being concentric circles or parallel straight-lines, for example, cones, inverse cones and inclined planes (Pan *et al*. 2004, Chirico *et al*. 2005). For these surfaces, the theoretical SCA value at every point along a given contour is constant and equal to the total upslope area of this contour divided by the contour length. Unfortunately, such terrain types are rare and the SCA value along contours is often variable in the real world.

Zhou and Liu (2002) proposed an ellipsoid, an inverse ellipsoid and a hyperbolic paraboloid to evaluate the performances of flow direction algorithms (Figure 1 and Table 1), respectively, simulating convex slope, concave slope and saddle surface with variable SCA along contours. From the mathematical definition of an artificial surface, theoretical SCA at every point can be analytically solved as the limit value of total contributing area (TCA) while the contour length (CL) tends to zero (Zhou and Liu 2002), that is,

Pan *et al.*'s (2004) model    Zhou and Liu's (2002) model



(a)

(b)

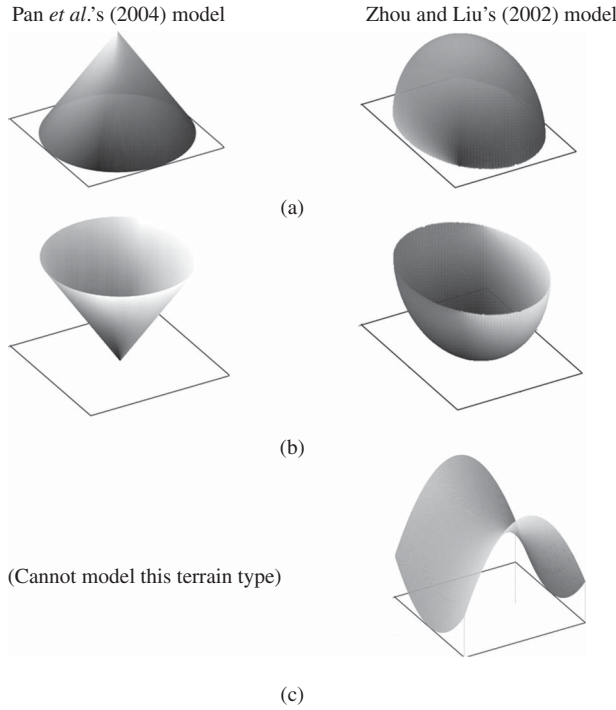(Cannot model this terrain type)

(c)

Figure 1.    Examples of artificial surfaces proposed by Pan *et al.* (2004) and Zhou and Liu (2002). (a) Convex slope (divergent flow), (b) concave slope (convergent flow) and (c) saddle slope.

Table 1.    Definitions and theoretical SCAs of artificial surfaces proposed by Zhou and Liu (2002).

| Surface | Model | Definition | Theoretical SCA[*],[**],[***] |
|---------|-------|-----------|------------------|
| Convex slope | Ellipsoid | $\frac{x^2}{a^2} + \frac{y^2}{b^2} + \frac{z^2}{c^2} = 1,$ $z > 0$ | $SCA = \frac{\sqrt{a_1^4 y_1^2 + b_1^4 x_1^2}}{a_1^2 + b_1^2}$ |
| Concave slope | Inverse ellipsoid | $\frac{x^2}{a^2} + \frac{y^2}{b^2} + \frac{z^2}{c^2} = 1,$ $z < 0$ | $SCA = \frac{\left(\frac{x_4}{x_1}\right)^{m+1} - 1}{a_1^2 + b_1^2} \sqrt{a_1^4 y_1^2 + b_1^4 x_1^2}, x_i \neq 0;$ |
| | | | $SCA = \frac{\left(\frac{y_4}{y_1}\right)^{1+1/m} - 1}{a_1^2 + b_1^2} \sqrt{a_1^4 y_1^2 + b_1^4 x_1^2}, x_i = 0$ |
| Saddle | Hyperbolic paraboloid | $\frac{x^2}{a^2} - \frac{y^2}{b^2} = \frac{z}{c},$ $-A < x, y < A,$ $(a \neq b)$ | $SCA = \frac{\left(\frac{\lvert x_1 \rvert}{A}\right)^{m-1} - 1}{b_1^2 - a_1^2} \sqrt{a_1^4 y_1^2 + b_1^4 x_1^2}$ |
| Straight slope | Plane | $z = ax + by + c,$ $-A < x, y < A$ | $SCA = \frac{A - x_1}{a} \sqrt{a^2 + b^2}$, where flow path intersects with $x = A$; |
| | | | $SCA = \frac{A - y_1}{b} \sqrt{a^2 + b^2}$, where flow path intersects with $y = A$ |

Notes: [*]$a_i$, $b_i$ denote the parameters of the surface model at point $(x_i, y_i)$.
[**]$m = \frac{a^2}{b^2}$.
[***]For the theoretical SCA of the concave slope, $(x_4, y_4)$ is the intersection point of the margin of the surface and the flow line ($y = Cont \cdot x^m$, where *Cont* denotes the constant) passing the point $(x_1, y_1)$.

$$SCA = \lim_{CL \to 0} \frac{TCA}{CL} \qquad (1)$$

TCA for a contour segment of a given CL can be recognised as the upslope area bounded by flow paths at the initial and terminal vertices of this segment of contour. The flow path is the trace line of the flow along the maximum hydraulic slope. The maximum hydraulic slope is estimated as the maximum downslope gradient. In this way, theoretical SCA of Zhou and Liu's (2002) artificial surfaces was analytically solved (Table 1).

To the best of our knowledge, the work of Zhou and Liu (2002) has hitherto presented the only existing method for creating artificial surfaces with variable SCA values along contours for evaluating flow direction algorithms. Artificial surfaces for more complex slope types, such as the Gauss synthetic surface (Zhou *et al.* 2006) and the general polynomial fitted function (Minár and Evans 2008), have also been proposed to evaluate the computation of local topographic attributes (e.g. slope gradient and curvature) or to analyse the land surface morphology. But theoretical SCA of these surfaces is hardly to be analytically solved for practical application in evaluating flow direction algorithms, because the difficulty in solving the theoretical SCA analytically increases dramatically for the artificial surfaces simulating complex surfaces.

However, the terrain types simulated by Zhou and Liu's (2002) artificial surfaces are still oversimplified and can rarely be used to simulate complex terrain types. Hill slopes similar to those considered in their simulations are rarely found in the real world. The maximum slope angle on the convex slope simulated by Zhou and Liu's (2002) ellipsoid surface is always 90°, whether or not the terrain condition simulated is low relief or high relief (further discussion is provided in Section 3). These convex slopes cannot be realistic. Similarly, the concave slopes simulated by Zhou and Liu's (2002) inverse ellipsoid surface are also unrealistically with a maximum slope angle being 90°. According to the definition of Zhou and Liu's (2002) saddle surface (Table 1 and Figure 1c), the elevation range of the simulated saddle surface has no limit until user assigns the boundaries arbitrarily. In this case, the theoretical SCA value at a given position on the simulated surface does not have a specific value, because it is influenced by the user-assigned boundaries. This is also unrealistic.

This article proposes a set of artificial surfaces with the theoretical SCA analytically solved; hence evaluating the performance of grid-based flow direction algorithms on complex terrain types.

## 2.  Basic idea

Performances of flow direction algorithms applied to complex terrain types should be evaluated using artificial surfaces (Zhou and Liu 2002). This is because complex terrain types, rather than simple terrain types, are commonplace in the real landscape. For example, slope is a complex terrain type because it often shows a smooth transition between slope positions, such as from a convex ridge top with low gradient, to a steeper planar slope and finally to a concave valley with low gradient (Qin *et al.* 2009). It is one of the most widespread terrain types in real landscapes. Existing methods cannot simulate this complex terrain type.

The sine and cosine functions could be applied in designing artificial surfaces for evaluating the performances of flow direction algorithms, for two reasons. First, the conceptual profile of a typical slope is similar to the curves of the sine and cosine functions. Thus,

complex terrain types could be simulated with artificial surfaces defined by sine and cosine functions. Second, if an artificial surface is defined with sine and cosine functions, it is possible to analytically solve the theoretical SCA value of this surface due to the simple functional form of the definition. Therefore, sine and cosine functions (or combinations thereof) are highly suited to model artificial surfaces. These artificial surfaces can simulate complex terrain types that are typical and widespread in real topography.

## 3.  A set of new artificial surface models

### 3.1.  *Artificial surfaces and their theoretical SCA*

We designed a set of new artificial surface models based on sine and cosine functions (named as sine–cosine models), which simulate the convex-centred slope, concave-centred slope, saddle-centred slope and straight-ridge slope, respectively. These four complex terrain types and their spatial combinations are widespread in real landscapes. The sine–cosine models and corresponding analytic solutions to the SCA equations are shown in Table 2. The detailed theoretical solutions to the SCA equations (Equation (1)) by following Zhou and Liu's (2002) method are not included in this article due to the limited length, and interested readers can demand these solutions by sending email to the corresponding author of this article.

Artificial surfaces created by sine–cosine models can simulate diverse terrain conditions with variable SCA values along the contours. Controlled by the spatial extent parameters *a* and *b* (Table 2), the artificial surfaces have variable spatial extent. The relief of the artificial surfaces created is also variable and is determined by specifying the relief parameter *c* (Table 2). Figure 2 shows examples of artificial surfaces created by the sine–cosine models and the corresponding theoretical SCA surfaces.

### 3.1.1.  *The convex-centred slope*

The *convex-centred slope* (Figure 2a), which is convex in the central part of the surface, is constructed from a cosine function. Starting from the summit point at the centre of the artificial surface, the slope changes gradually from convex to concave along the profile. This complex terrain type not only includes the simple convex terrain type simulated by the ellipsoid surface in Zhou and Liu (2002), but also simulates the general spatial context of convex terrain in real topography (the transition from convexity to concavity).

The maximum slope angle of the convex-centred artificial surfaces varies when the relief of the artificial surface varies. The greater the relief (achieved by increasing the relief parameter), the larger the maximum slope angle. The position with the maximum slope gradient is in the middle of the back slope of the convex-centred artificial surface. In this position, the profile curvature is zero and from here to the summit, the profile curvature is convex with a value that gradually increases to a maximum (i.e. $c\pi^2/2a^2$). The greater is the relief, the larger is the maximum of the profile curvature. From this middle position to the lowest position, the profile curvature of the convex-centred artificial surface gradually decreases to a minimum (i.e. $-c\pi^2/2a^2$). The greater the relief, the lower the minimum of the profile curvature.

The characteristics shown in the convex-centred artificial surfaces are common where convex terrain occurs within real topography, but cannot be simulated by the ellipsoid model in Zhou and Liu (2002). No matter how the relief in the ellipsoid surface proposed by that model is simulated, the maximum slope angle is always 90° and located at the

Table 2. Definitions and theoretical SCAs of artificial surfaces based on the sine–cosine models proposed in this study.

| Artificial surface | Model | Definition | Theoretical SCA |
|---|---|---|---|
| Convex-centred slope | Cosine | $z = \frac{c}{2} + \frac{c}{2} \cdot \cos\left(\pi\sqrt{\frac{x^2}{a^2}+\frac{y^2}{b^2}}\right)$, $\frac{x^2}{a^2}+\frac{y^2}{b^2} \leq 1$ | $SCA = \frac{\sqrt{a^4 y^2 + b^4 x^2}}{a^2+b^2}$ |
| Concave-centred slope* | Cosine | $z = \frac{c}{2} - \frac{c}{2} \cdot \cos\left(\pi\sqrt{\frac{x^2}{a^2}+\frac{y^2}{b^2}}\right)$, $\frac{x^2}{a^2}+\frac{y^2}{b^2} \leq 1$ | $SCA = \frac{\left(\frac{x_4^{\frac{1+m}{}}}{x_1^{\frac{1+m}{}}}-1\right)}{a^2+b^2}\sqrt{a^4 y_1^2 + b^4 x_1^2}$, $x_1 \neq 0$; and $SCA = \frac{\left(\frac{y_4^{\frac{1+1/m}{}}}{y_1^{\frac{1+1/m}{}}}-1\right)}{a^2+b^2}\sqrt{a^4 y_1^2 + b^4 x_1^2}$, $x_1 = 0$, where $m = \frac{a^2}{b^2}$ |
| Saddle-centred slope** | Product of two sine functions | $z = \frac{c}{2} + \frac{c}{2} \cdot \sin\left(\frac{\pi}{a}x\right) \cdot \sin\left(\frac{\pi}{a}y\right)$, $-a \leq x, y \leq a$ | $SCA = \frac{a}{\pi}\sqrt{\tan^2\left(\frac{\pi}{a}x_1\right) + \tan^2\left(\frac{\pi}{a}y_1\right)} \cdot \ln\left(\frac{\cos\left(\frac{\pi}{a}y_1\right)+\cos\left(\frac{\pi}{a}x_1\right)}{\sin\left(\frac{\pi}{a}x_1+\frac{\pi}{a}y_1\right)}\right)$, where point $(x_1,y_1)$ meets $0 < x_1, y_1 < \frac{a}{2}, y_1 \leq x_1$; $SCA = \frac{a}{\pi}\sqrt{\tan^2\left(\frac{\pi}{a}x_1\right) + \tan^2\left(\frac{\pi}{a}y_1\right)} \cdot \ln\left(\frac{\sin\left(\frac{\pi}{a}x_1-\frac{\pi}{a}y_1\right)}{\cos\left(\frac{\pi}{a}y_1\right)-\cos\left(\frac{\pi}{a}x_1\right)}\right)$, where point $(x_1,y_1)$ meets $0 < x_1 < \frac{a}{2}, -\frac{a}{2} < y_1 < 0, y_1 > -x_1$; $SCA = \frac{a}{\pi} \cdot \frac{1-\sin\left(\frac{\pi}{a}y_1\right)}{\cos\left(\frac{\pi}{a}y_1\right)}$, where $x_1 = \frac{a}{2}, -\frac{a}{2} < y_1 < \frac{a}{2}$; $SCA = 0$ at points $(0,0)$ and $\left(\frac{a}{2}, \frac{a}{2}\right)$; $SCA = +\infty$ where $y_1 = -x_1, -\frac{a}{2} <= y_1 < 0$ |
| Straight-ridge slope *** | Cosine | $z = \frac{c}{2} + \frac{c}{2} \cdot \cos\left(\frac{\pi}{a} \cdot \frac{|\tan\theta \cdot x - y|}{\sqrt{\tan^2\theta+1}}\right)$, $\left(-\frac{l}{2}\cos\theta \leq x \leq \frac{l}{2}\cos\theta,\right.$ $\left.-\frac{l}{2}\sin\theta \leq y \leq \frac{l}{2}\sin\theta, \frac{|\tan\theta \cdot x - y|}{\sqrt{\tan^2\theta+1}} \leq a\right)$ | $SCA = \frac{|\tan\theta \cdot x - y|}{\sqrt{\tan^2\theta+1}}$ |

Notes: *For the theoretical SCA for the artificial concave-centred slope, $(x_4,y_4)$ is the intersection point of the margin of the surface and the flow line ($y = Cont \cdot x^m$, where $Cont$ denotes the constant) passing the point $(x_1,y_1)$.

**For the artificial surface of the saddle-centred slope, the theoretical SCA on a point in the comparison domain without being given directly is referred to the theoretical SCA on the point $(x_1,y_1)$ which meets $y_1 - x_1 \leq 0, y_1 + x_1 \geq 0, x_1 \leq \frac{a}{2}$ and is the symmetry point of the given point.

***For the artificial surface of the straight-ridge slope, the parameters $\theta$ and $l$ are set to control the direction and the length of the simulated ridge, respectively.
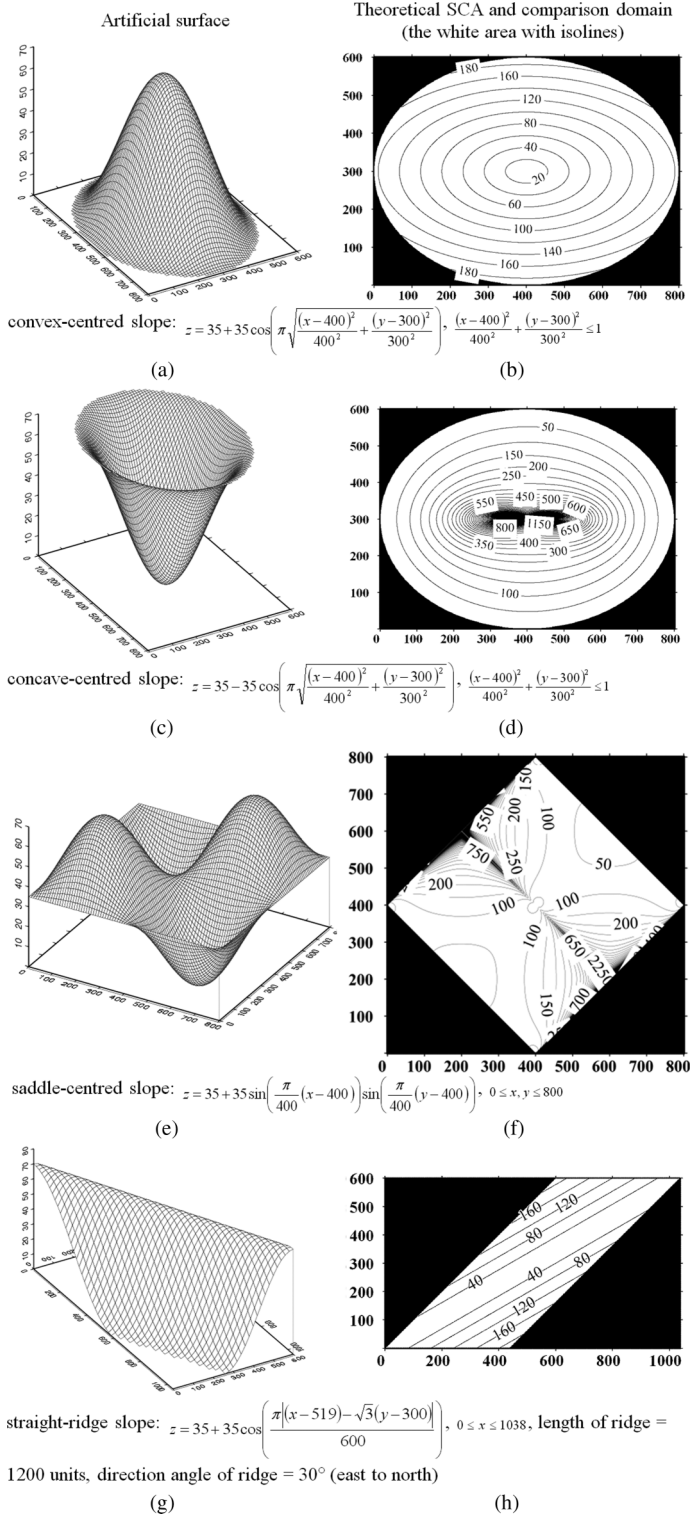
Figure 2. Examples of artificial surfaces proposed in this article (see Table 2), the theoretical SCA surfaces and the comparison domains.

lowest position at the foot of the slope. The maximum of the profile curvature (i.e. $a/c^2$) is also always located at the lowest position. The minimum of the profile curvature is always located at the summit and is a non-zero positive value (i.e. $c/a^2$). Although Zhou and Liu (2002) suggested using part of the ellipsoid surface instead of the whole artificial surface in practice, the maximum slope angle in such a case is again located at the lowest position at the foot of the slope. Thus, the slope is still unrealistic. This shows that the convex-centred slope can simulate the convex terrain types encountered in real topography more realistically than the ellipsoid surface proposed in Zhou and Liu (2002).

### 3.1.2. The concave-centred slope

The *concave-centred slope* (Figure 2c) constructed by a cosine function, which is concave in the central part of the surface, is an inverse version of the convex-centred slope. Therefore, the results of comparable analysis between the concave-centred slope and Zhou and Liu's (2002) inverse ellipsoid surface are similar to that between the convex-centred slope and the ellipsoid surface. The complex terrain type simulated by the concave-centred surface includes not only the simple concave terrain type represented by the inverse ellipsoid surface in Zhou and Liu (2002), but also the general spatial context of concave terrain in real topography. The concave-centred slope is more realistic than it defined in the inverse ellipsoid model.

### 3.1.3. The saddle-centred slope

The *saddle-centred slope* (Figure 2e) is constructed from the product of two sine functions. The saddle point is at the centre of this surface. On this artificial surface, the ridge line shows a smooth transition from convex to concave as position changes from the summit to the saddle point. In the direction orthogonal to the ridge line, the profile originating from the saddle point shows a smooth transition from convex to concave when moving from the saddle point to the bottom of the depression. The spatial context of the saddle simulated by the saddle-centred slope has a finite range of elevation that is unaffected by the user-assigned boundaries. The theoretical SCA value at a given position has a specific, finite value that is unaffected by the boundaries assigned arbitrarily by the user. This situation is similar to that found in real saddle terrain but cannot be simulated by Zhou and Liu's (2002) hyperbolic paraboloid surface (as we described in Section 1).

### 3.1.4. The straight-ridge slope

The *straight-ridge slope* (Figure 2g) is constructed from a cosine function. A straight ridge lies along the middle of the artificial surface. All contours are straight and parallel to the ridge. Both parts of any one profile intersected by the straight ridge are symmetrical. There is a smooth transition from convex to concave when moving from ridge to valley along the profile. Compared with the simple planar terrain simulated by Zhou and Liu's (2002) planar surface, the straight-ridge slope can simulate the general spatial context of a terrain type with parallel flow and thus is more typical of real topography.

### 3.2. Comparison domains for artificial surfaces

We imported the concepts of the computational domain, influence domain and comparison domain proposed by Pan *et al*. (2004) for applying the artificial surfaces proposed above to

the performance evaluation of flow direction algorithms. The computational domain of an artificial surface is defined as the region in which we apply a flow direction algorithm for computing SCA, that is, the spatial extent of the artificial surface. The influence domain is defined as the area inside the computational domain that receives a flow contribution from the lateral boundaries. The comparison domain, which is the area inside the computational domain but outside the influence domain, receives no flow contribution from the boundaries (Pan *et al*. 2004). The performances of flow direction algorithms are only evaluated in the comparison domain, thus avoiding the influence of the user-assigned boundaries on the computed SCA.

The comparison domains of the four types of artificial surfaces proposed in this article are shown in Figure 2b, d, f, and h as the white areas with isolines in the extent of artificial surfaces. For the convex-centred slope and concave-centred slope, the comparison domain is the same as the computational domain (Figure 2a–d). For the saddle-centred slope, we narrowed the range of the comparison domain by assigning the summit as the endpoint of the ridge line in the comparison domain. The point at which the profile originating from the saddle point in the direction orthogonal to that of the ridge line reaches the bottom of the depression was defined as being the endpoint in the comparison domain (Figure 2f), thereby focusing attention on the saddle part of the saddle-centred slope.

## 4.   Application

In this section, the proposed artificial surfaces are applied to evaluate the performances of grid-based flow direction algorithms, so that the feasibility of the proposed artificial surfaces can be instantiated.

### 4.1.   *Experimental design*

Two artificial surface examples having different reliefs but the same spatial extents were created for each type of proposed artificial surfaces. The two relief grades represent high-relief and low-relief topography and were defined by setting the relief parameter $c$ to be 70 and 20 m, respectively. For the convex-centred slope and concave-centred slope artificial surface types, the spatial extents of the artificial surfaces were defined as $800 \times 600$ by setting the parameters $a = 400$ and $b = 300$ (in units of meters, being consistent with that of the relief parameter). For the saddle-centred slope, the spatial extents of the artificial surfaces were defined as 800 m $\times$ 800 m by setting the parameter $a = 400$ m. The artificial surfaces for the straight-ridge slope were created by setting the parameter $a = 300$ m. The ridge was oriented at 30° (east to north) and had a length of 1200 m. Although the parameter settings are arbitrary, we suppose that there is less loss of generality. Figure 2 shows the high-relief examples of proposed artificial surfaces and the corresponding theoretical SCA surfaces. The theoretical SCA surfaces were created by equations in Table 2.

The artificial DEMs were created by sampling the artificial surface examples at a series of resolutions (i.e. 1, 5, 10 and 20 m), for a quantitative and multiple-scale assessment of flow direction algorithms. The series of resolutions used in this study are comparable with those used in many applications at finer scale (e.g. Kienzle 2004, Erskine *et al*. 2007, Qin *et al*. 2011). We think the grid size coarser than 20 m is not sufficient for representing the continuous change of the artificial surface examples in raster manner and performing statistical analysis in this study.

These artificial DEMs were applied in the error assessment of four representatives of grid-based flow direction algorithms, namely, D8 (O'Callaghan and Mark 1984), D-inf (Tarboton 1997), FD8 (Quinn *et al*. 1991) and MFD-md (Qin *et al*. 2007). D8 is a classic single flow direction algorithm in which all water from a cell flow into one and only one neighbouring cell with the steepest downslope. It has been implemented in many widely used GIS software packages, such as ArcGIS™ (Environmental Systems Research Institute, Inc., www.esri.com).

D-inf, as one of the most frequently used flow direction algorithms, determines the flow direction as the direction of the steepest descent on the eight planar triangular facets formed between the cell of interest and its neighbouring cells (Tarboton 1997). In D-inf, the flow direction angle is represented as a continuous quantity between 0 and $2\pi$. Flow from each cell drains to at most two neighbouring cells. D-inf algorithm has been implemented in the TauDEM© tool developed by Prof. David G. Tarboton (http://hydrology.usu.edu/taudem/taudem3.1/).

FD8 and MFD-md algorithms are representatives of multiple flow direction (MFD) algorithms with a fixed-flow-exponent scheme and adaptive-flow-partition scheme, respectively (Qin *et al*. 2007). In the FD8 algorithm, flow from a cell drains into all downslope neighbouring cells based on the flow partition scheme, as follows:

$$d_i = \frac{(\tan \beta_i)^p \times L_i}{\sum_{j=1}^{8} (\tan \beta_j)^p \times L_j} \tag{2}$$

where $d_i$ is the proportion of flow draining into the *i*-th neighbouring cell, $\tan \beta_i$ is the slope gradient between the central cell and its *i*-th neighbouring cell, the exponent $p$ is the flow partition exponent ($p = 1$ in FD8) and $L_i$ is the effective contour length of the *i*-th neighbouring cell. The value of $L_i$ is 0.5 for downslope cells in cardinal directions, 0.354 for downslope cells in the diagonal directions and 0 for non-downslope cells (Quinn *et al*. 1991). In the MFD-md algorithm, a linear function of maximum downslope gradient is used to replace the flow partition exponent $p$ in Equation (2) to model the flow partition, making the algorithm adaptive to the local terrain conditions (Qin *et al*. 2007).

When each artificial DEM was sampled from the proposed artificial surface, a theoretical SCA grid was also created by sampling the corresponding theoretical SCA surface at the same resolution as that of the artificial DEM. Thus, the errors in the flow direction algorithm can be quantitatively calculated by

$$E_i = SCA_i - SCA_i^{\text{true}} \tag{3}$$

where $E_i$ is the error in the flow direction algorithm at the *i*-th cell, and $SCA_i^{\text{true}}$ and $SCA_i$ are the theoretical SCA and the computed SCA for the *i*-th cell, respectively.

### 4.2.  *Aspects of evaluation*

The performance of flow direction algorithm applied to the proposed artificial DEMs can be evaluated from three aspects. First, the errors in the tested flow direction algorithms at different DEM resolutions can be quantitatively assessed using the root mean square error (RMSE), mean error (ME) and standard deviation (SD). Second, the cumulative frequency distribution of error in the flow direction algorithms applied to each artificial DEM can be computed for the evaluation of the systematic bias of each tested flow direction algorithm.

Furthermore, the map of the error in each tested flow direction algorithm can be used for a spatially explicit evaluation of the error in the flow direction algorithm. Note that the evaluation by each artificial DEM is made only for the cells completely in the corresponding comparison domain.

### 4.3. Results

Table 3 lists the RMSE, ME and SD when applying D8, D-inf, FD8 and MFD-md to the proposed artificial low-relief DEMs at a series of resolutions. The table also shows that each flow direction algorithm yielded much lower errors for convex-centred or straight-ridge slope than for concave-centred or saddle-centred slope. D8 performed worst at all tested resolutions.

For convex-centred slope, RMSE values from other tested flow direction algorithms are much lower than from D8 (Table 3). MFD-md performed best at the resolutions of 1 and 5 m. Under the convex-centred DEMs with resolutions of 10 and 20 m, RMSE from MFD-md is slightly higher than that from D-inf but still lower than that from FD8 or D8. When the resolution of the artificial DEM is progressively coarsened from 1 to 20 m, RMSE values from MFD-md and FD8 increase slightly and constantly. Contrarily, RMSE values from D8 and D-inf decrease slowly and constantly with coarsening the DEM resolution.

For concave-centred slope, the RMSE values from D-inf, FD8 and MFD-md are very close. FD8 performed best under the 1-m DEM when D-inf performed best under the concave-centred DEMs with other resolutions. RMSE from each tested flow direction algorithm decreases constantly when the DEM resolution gets coarser. The level of decrease in RMSE from D8 is much higher than those from D-inf, FD8 and MFD-md.

For saddle-centred slope with all tested resolutions, MFD-md performed best and D8 performed worst. RMSE from FD8 is slightly higher than that from MFD-md when RMSE from D-inf is higher than that from FD8. RMSE from each tested flow direction algorithm decreases constantly when the DEM resolution gets coarser. The level of decrease in RMSE from D8 is much higher than that from D-inf, FD8 or MFD-md. This situation is similar to that for concave-centred slope.

For straight-ridge slope, MFD-md performed best under the DEMs with almost all tested resolution. Only under the DEM with 20 m resolution, RMSE from MFD-md is slightly higher than that from D-inf but still much lower than that from FD8 or D8. When the resolution gets coarser, RMSE from MFD-md, FD8 and D8 increase slightly and constantly. Contrarily, RMSE from D-inf decreases slowly and constantly with coarsening the DEM resolution.

Table 4 lists the RMSE, ME and SD when applying each flow direction algorithm to the artificial high-relief DEMs at a series of resolutions. The comparison between Tables 3 and 4 shows that with coarsening the DEM resolution, each tested flow direction algorithm has the same error-changing trends under different reliefs. For D8, D-inf and FD8, the RMSE values under high-relief terrains are almost the same as those under the low-relief DEMs. The only exception is under the saddle-centred DEMs with 1 m resolution, which RMSE values from D8, D-inf and FD8 applied with high relief are higher than the corresponding RMSE values with low relief. For MFD-md algorithm, RMSE values under artificial high-relief DEMs are generally lower than under the corresponding low-relief DEMs, although the case of the saddle-centred DEM with 1 m resolution and the cases of the straight-ridge DEMs with resolutions of 1 and 5 m show the opposite situation.

The above quantitative assessment with the proposed artificial DEMs with different reliefs at a series of resolutions shows that the applicable conditions (e.g. terrain condition

Table 3. RMSE, ME and SD from the D8, D-inf, FD8 and MFD-md algorithms applied to artificial DEMs with low relief (relief = 20 m) created from the proposed artificial surfaces.

| Flow direction algorithm | Grid size (m) | Convex-centred DEM | | | Concave-centred DEM | | | Saddle-centred DEM | | | Straight-ridge DEM | | |
|---|---|---|---|---|---|---|---|---|---|---|---|---|---|
| | | RMSE | ME | SD | RMSE | ME | SD | RMSE | ME | SD | RMSE | ME | SD |
| D8 | 1 | 65.8 | −14.3 | 64.3 | 1906.8 | −22.2 | 1906.7 | 1354.2 | 18.0 | 1354.0 | 24.3 | −20.0 | 13.8 |
| | 5 | 63.8 | −15.6 | 61.9 | 815.2 | −17.6 | 815.0 | 616.3 | 41.8 | 614.9 | 25.3 | −21.4 | 13.5 |
| | 10 | 62.3 | −17.5 | 59.7 | 540.1 | −15.5 | 539.9 | 414.6 | 47.5 | 411.9 | 26.6 | −23.1 | 13.3 |
| | 20 | 58.0 | −22.6 | 53.5 | 351.6 | −11.8 | 351.4 | 285.5 | 51.8 | 280.7 | 29.6 | −26.4 | 13.5 |
| D-inf | 1 | 14.2 | −12.7 | 6.3 | 506.0 | −16.8 | 505.7 | 403.2 | −3.9 | 403.2 | 14.4 | −11.7 | 8.5 |
| | 5 | 11.6 | −9.8 | 6.3 | 327.8 | −8.1 | 327.7 | 324.6 | 25.9 | 323.6 | 12.5 | −9.5 | 8.1 |
| | 10 | 9.4 | −6.5 | 6.7 | 273.6 | −1.1 | 273.6 | 229.4 | 34.1 | 226.8 | 10.5 | −6.8 | 7.9 |
| | 20 | 7.6 | −0.2 | 7.6 | 228.1 | 12.1 | 227.7 | 166.3 | 45.5 | 160.0 | 8.8 | −1.2 | 8.7 |
| FD8 | 1 | 11.7 | 10.4 | 5.4 | 500.3 | 25.3 | 499.7 | 220.8 | 45.4 | 216.1 | 10.8 | 9.0 | 6.0 |
| | 5 | 14.0 | 12.8 | 5.8 | 350.7 | 35.2 | 348.9 | 183.0 | 56.2 | 174.1 | 12.4 | 10.9 | 5.9 |
| | 10 | 16.6 | 15.5 | 6.1 | 300.3 | 43.4 | 297.1 | 156.4 | 60.1 | 144.4 | 14.4 | 13.3 | 5.7 |
| | 20 | 21.8 | 20.8 | 6.2 | 259.8 | 58.7 | 253.1 | 135.9 | 66.4 | 118.6 | 18.9 | 18.2 | 5.2 |
| MFD-md | 1 | 6.9 | 4.7 | 5.1 | 507.0 | 12.6 | 506.8 | 213.1 | 36.1 | 210.0 | 2.4 | 2.3 | 0.6 |
| | 5 | 8.7 | 7.0 | 5.2 | 349.5 | 22.1 | 348.9 | 176.4 | 46.7 | 170.1 | 4.3 | 4.2 | 0.6 |
| | 10 | 11.0 | 9.7 | 5.1 | 297.8 | 30.0 | 296.3 | 149.0 | 50.4 | 140.2 | 6.8 | 6.8 | 0.6 |
| | 20 | 15.7 | 14.9 | 4.7 | 256.6 | 44.7 | 252.6 | 127.6 | 56.8 | 114.3 | 12.0 | 11.9 | 1.5 |

Note: For the convex-centred and concave-centred DEMs, the numbers of cells in comparison domain used for calculating the statistics are 374180, 14520, 3484 and 804, respectively, at 1, 5, 10 and 20 m resolution. The numbers of cells in comparison domain of the saddle-centred DEMs are 319200, 12640, 3120, and 760, respectively, at 1, 5, 10 and 20 m resolution. The numbers of cells in comparison domain of the straight-ridge DEMs are 260130, 9794, 2262 and 476, respectively, at 1, 5, 10 and 20 m resolution.

Table 4. RMSE, ME and SD from the D8, D-inf, FD8 and MFD-md algorithms applied to artificial DEMs with high relief (relief = 70 m) created from the proposed artificial surfaces.

| Flow direction algorithm | Grid size (m) | Convex-centred DEM | | | Concave-centred DEM | | | Saddle-centred DEM | | | Straight-ridge DEM | | |
|---|---|---|---|---|---|---|---|---|---|---|---|---|---|
| | | RMSE | ME | SD | RMSE | ME | SD | RMSE | ME | SD | RMSE | ME | SD |
| D8 | 1 | 65.7 | −14.3 | 64.1 | 1906.8 | −22.2 | 1906.7 | 1456.6 | 27.7 | 1456.0 | 24.3 | −20.0 | 13.8 |
| | 5 | 63.8 | −15.6 | 61.9 | 815.2 | −17.6 | 815.0 | 616.3 | 41.8 | 614.9 | 25.3 | −21.4 | 13.5 |
| | 10 | 62.3 | −17.5 | 59.7 | 540.1 | −15.5 | 539.9 | 414.6 | 47.5 | 411.9 | 26.2 | −22.7 | 13.1 |
| | 20 | 58.0 | −22.6 | 53.5 | 351.6 | −11.8 | 351.4 | 285.5 | 51.8 | 280.7 | 29.6 | −26.4 | 13.5 |
| D-inf | 1 | 14.1 | −12.7 | 6.3 | 505.4 | −16.8 | 505.1 | 617.6 | 5.4 | 617.6 | 14.4 | −11.7 | 8.5 |
| | 5 | 11.6 | −9.8 | 6.3 | 327.8 | −8.1 | 327.7 | 329.0 | 26.4 | 327.9 | 12.5 | −9.5 | 8.1 |
| | 10 | 9.4 | −6.5 | 6.7 | 273.6 | −1.1 | 273.6 | 229.2 | 34.0 | 226.7 | 10.3 | −6.6 | 7.8 |
| | 20 | 7.6 | −0.2 | 7.6 | 228.1 | 12.1 | 227.7 | 166.3 | 45.5 | 159.9 | 8.8 | −1.2 | 8.7 |
| FD8 | 1 | 11.7 | 10.4 | 5.4 | 501.0 | 25.3 | 500.3 | 261.6 | 51.1 | 256.6 | 10.8 | 9.0 | 6.0 |
| | 5 | 14.0 | 12.8 | 5.8 | 350.7 | 35.2 | 348.9 | 183.0 | 56.2 | 174.2 | 12.4 | 10.9 | 5.9 |
| | 10 | 16.6 | 15.5 | 6.1 | 300.3 | 43.4 | 297.1 | 156.4 | 60.1 | 144.4 | 14.2 | 13.1 | 5.6 |
| | 20 | 21.8 | 20.8 | 6.2 | 259.8 | 58.7 | 253.1 | 135.9 | 66.4 | 118.6 | 18.9 | 18.2 | 5.2 |
| MFD-md | 1 | 5.3 | −0.8 | 5.3 | 501.7 | 0.0 | 501.7 | 248.0 | 29.9 | 246.2 | 7.0 | −4.6 | 5.4 |
| | 5 | 5.6 | 1.4 | 5.4 | 345.6 | 9.2 | 345.5 | 165.9 | 34.4 | 162.3 | 5.7 | −2.5 | 5.1 |
| | 10 | 6.6 | 4.1 | 5.2 | 295.4 | 16.7 | 294.9 | 136.8 | 38.1 | 131.4 | 4.9 | 0.2 | 4.9 |
| | 20 | 10.4 | 9.3 | 4.7 | 254.6 | 30.9 | 252.7 | 115.0 | 45.1 | 105.8 | 7.5 | 5.5 | 5.1 |

Note: The number of cells in comparison domain used for calculating the statistics is the same as it is for the corresponding low-relief case.

and resolution of DEM) of the tested flow direction algorithms are different. The MFD-md algorithm generally performed better under simulated terrain conditions than D-inf, FD8 or D8.

The cumulative frequency distributions of errors from the flow direction algorithms were computed for the artificial DEMs with 1 m resolution for a given type of proposed artificial surface under different reliefs (Figure 3). Figure 3 shows that the cumulative frequency distributions of errors from D8, D-inf and FD8 are invariant under different reliefs. These results are consistent with the steepest downslope-direction characteristic of D8 and D-inf and the fixed-flow-partition characteristic of FD8, respectively. The number of cells in which D8 yields a negative error is obviously larger than the number of cells in which D8 yields a positive error. This means that the D8 algorithm tends to underestimate the SCA. D-inf algorithm also tends to underestimate the SCA, but with a much lesser degree than D8 algorithm. FD8 yields a positive error in almost all cells; so the FD8 algorithm tends to overestimate the SCA.

Figure 3 shows that MFD-md yields error near zero in more cells than D8, D-inf or FD8. This indicates that MFD-md performs better than D8, D-inf or FD8. As the terrain of the artificial DEMs varies from low relief to high relief, the cumulative frequency distribution of errors from MFD-md shows a transition between those of FD8 and D-inf (Figure 3). This means that MFD-md performs more similarly to FD8 in low-relief terrains and more similarly to D-inf in high-relief terrains. The performance of MFD-md with the artificial DEMs is consistent with the properties of MFD-md, which is adaptive to the local terrain conditions as was also shown in an application using a real DEM of a watershed (Qin *et al*. 2007). The cumulative frequency distributions of errors from the flow direction algorithms applied with other tested resolutions show similar phenomena. Limited by the length, those with other tested resolutions are not listed in this article.

The map of error in each tested flow direction algorithm is available for a spatially explicit and detailed evaluation on the occurrence of error. The error maps of flow direction algorithms tested with the convex-centred DEMs with 1 m resolution (Figure 4a) show that the error maps for D8, D-inf and FD8 are invariant under different reliefs, while the error maps for the MFD-md algorithm vary between reliefs of the artificial DEM. The magnitude of error in D8 is much larger than that in D-inf or MFD. In addition, the error from D8 shows a regular change between positive and negative in different directions from the summit of the convex-centred slope (Figure 4a). This is obviously an effect of the error accumulation originating from the single-flow-direction scheme in D8, which is avoided in the other tested flow direction algorithms.

Generally, the error from D-inf, FD8 and MFD-md is higher at the lower positions of the convex-centred slope than at the upper positions (Figure 4a). Over most of the area, the D-inf algorithm underestimates the SCA when FD8 overestimates the SCA. An effect similar to that with FD8 was seen with the MFD-md algorithm applied with low relief, but to a lesser degree. The overestimate of the computed SCA by the MFD-md algorithm is further moderated when MFD-md was applied to a high-relief DEM (Figure 4a). Some areas with negative error in the MFD-md algorithm are revealed where D8 has negative error. These characteristics confirm the key features of MFD-md, in particular its ability to adapt to the local terrain conditions, which results in MFD-md performing more similarly to FD8 in low-relief terrains and more similarly to D8 under high-relief terrains. The error maps of the flow direction algorithms applied with other tested resolutions show similar characteristics. Limited by the length, those maps are not given in this article.

The error maps of flow direction algorithms tested with the concave-centred, saddle-centred slope and straight-ridge DEMs with 1 m resolution are shown in Figure 4b, c,
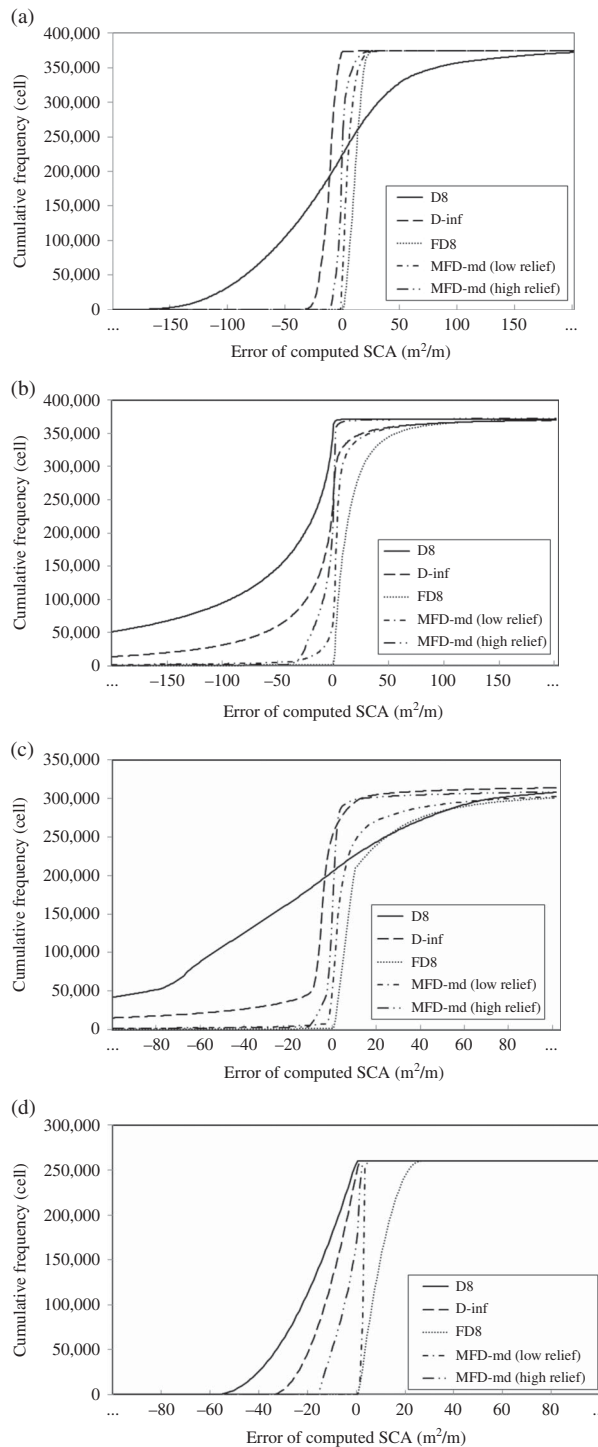
Figure 3.   Cumulative frequency distributions of errors from D8, D-inf, FD8 and MFD-md algorithms applied to artificial DEMs (grid size = 1 m) created from the proposed artificial surfaces. (MFD-md (low relief) and MFD-md (high relief) in the legend means the MFD-md algorithm applied to the low-relief ($c = 20$) case and the high-relief ($c = 70$) case, respectively). (a) Convex-centred DEM, (b) concave-centred DEM, (c) saddle-centred slope DEM and (d) straight-ridge DEM.
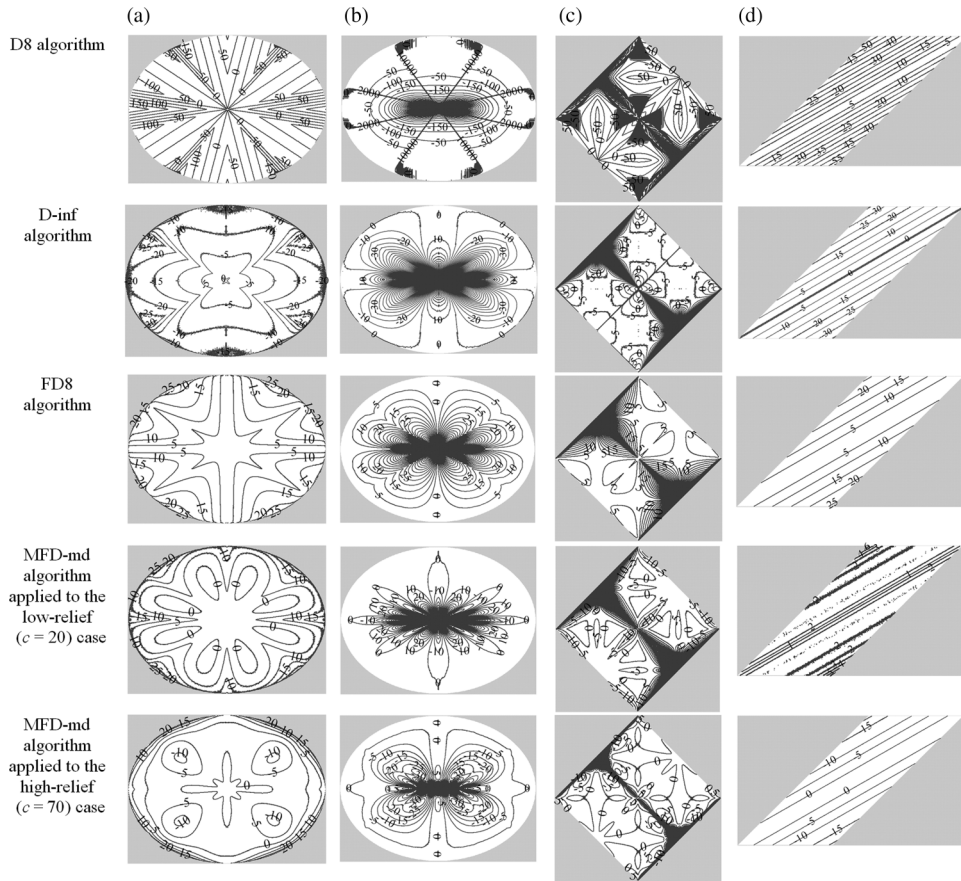
Figure 4. Maps of the error in each tested flow direction algorithm when applied to the proposed artificial DEMs (grid size = 1 m) created from the proposed artificial surfaces. (a) Convex-centred DEM, (b) concave-centred DEM, (c) saddle-centred slope DEM and (d) straight-ridge DEM.

and d, respectively. Similarly, Figure 4b, c, and d show that the magnitude of error in D8 is much larger than that in D-inf, FD8 or MFD-md. Over most of the area, the D-inf algorithm underestimates the SCA when FD8 overestimates the SCA. The MFD-md algorithm, due to its ability to adapt to the local terrain conditions, performed better under simulated terrain types than FD8, D-inf or D8, which has invariant error maps under different reliefs of a specific surface simulated. The error from D8 tested with the concave-centred slope shows a strong bias towards specific directions (Figure 4b). The information gained from the spatially explicit error mapping is valuable not only for the evaluation of the performance of a specific flow direction algorithm but also for a potential improvement of the algorithm (e.g. Zhan *et al*. 2012).

## 5.   Discussion and conclusions

Existing artificial surfaces developed for evaluating the performances of grid-based flow direction algorithms only simulate oversimplified terrain types which are very uncommon in real topography and are unrealistic. This article proposed a set of new artificial surfaces

simulating the complex terrain types which incorporate both the simple terrain types and their spatial context. This is valuable because the complex terrain types simulated are typical and widespread in real topography. Therefore, conclusions of algorithm performance drawn from assessments based on the proposed artificial surfaces have wider applicability and thus are more convincing for guiding the application of algorithm than those based on existing artificial surfaces for evaluating flow direction algorithms.

As shown in this study, a multiple-scale analysis on the performance of flow direction algorithms can be made based on the DEMs created by sampling the proposed artificial surfaces at a range of resolutions. The error maps produced, when the proposed artificial DEMs are applied to flow direction algorithms, are available to a spatially explicit and detailed discussion on the performance of the tested algorithms. Results of testing four representative flow direction algorithms with the proposed artificial surfaces show that MFD-md generally yielded lower error under simulated terrain conditions than D8, D-inf and FD8. D8 performed worst in the test. MFD-md performed more similarly to FD8 in low-relief terrains and more similarly to D-inf in high-relief terrains. Over most of the area, D-inf underestimated the SCA when FD8 overestimated the SCA.

It should be noted that the terrains simulated by the proposed artificial surfaces are smooth slope surfaces, as with other artificial surfaces. Thus, the evaluation of the flow direction algorithms is mainly focused on their performance for slope surfaces (including flow-initiation positions, such as ridges), not their performance in channels. We believe this is appropriate because of two aspects. First, the main difference between the SCA computed by different flow direction algorithms is along ridges and side slopes, and not in the more convergent terrain (such as channels) (Erskine *et al.* 2006). Second, accurate spatial distributions of SCA or other SCA-based topographic attributes for hill slopes are important in a number of terrain-related applications, especially at fine scales (Hengl and Reuter 2009). Thus, evaluation of the performance of flow direction algorithms on hill slopes is appropriate with the artificial surfaces. It should also be noted that the evaluation result with artificial surfaces is scale specific because of not only the spatial extents of the simulated slope surfaces, but also the resolution(s) of the artificial DEMs.

It is also possible that the proposed artificial surfaces could be used to evaluate the performances of algorithms computing the SCA-based topographic attributes (such as topographic wetness index and stream power index). Clearly, more work is needed to confirm the utility of these artificial surfaces in this context.

## References

Chirico, G.B., *et al.*, 2005. On the definition of the flow width for calculating specific catchment area patterns from gridded elevation data. *Hydrological Processes*, 19, 2539–2556.

Costa-Cabral, M.C. and Burges, S.J., 1994. Digital elevation model networks (DEMON): a model of flow over hillslopes for computation of contributing and dispersal areas. *Water Resources Research*, 30, 1681–1692.

Erskine, R.H., *et al*., 2006. Comparison of grid-based algorithms for computing upslope contributing area. *Water Resources Research*, 42 (W09416), 1–9. doi:10.1029/2005WR004648.

Erskine, R.H., *et al*., 2007. Digital elevation accuracy and grid cell size: effects on estimated terrain attributes. *Soil Science Society of America Journal*, 71, 1371–1380.

Freeman, T.G., 1991. Calculating catchment area with divergent flow based on a regular grid. *Computers & Geosciences*, 17, 413–422.

Gallant, J.C. and Hutchinson, M.F., 2011. A differential equation for specific catchment area. *Water Resources Research*, 47 (W05535), 1–14. doi:10.1029/2009WR008540.

Hengl, T. and Reuter, H.I., eds., 2009. *Geomorphometry: concepts, software, applications*. Amsterdam: Elsevier.

Kienzle, S., 2004. The effect of DEM raster resolution on first order, second order and compound terrain derivatives. *Transactions in GIS*, 8, 83–111.

Li, Z., Zhu, Q., and Gold, C., 2005. *Digital terrain modeling: principles and methodology*. Boca Raton, FL: CRC Press.

Minar, J. and Evans, I.S., 2008. Elementary forms for land surface segmentation: the theoretical basis of terrain analysis and geomorphological mapping. *Geomorphology*, 95, 236–259.

Moore, I.D., *et al*., 1991. Digital terrain modeling: a review of hydrological, geomorphological, and biological applications. *Hydrological Processes*, 5, 3–30.

O'Callaghan, J.F. and Mark, D.M., 1984. The extraction of drainage networks from digital elevation data. *Computer Vision, Graphics, and Image Processing*, 28, 323–344.

Pan, F., *et al*., 2004. A comparison of geographical information system-based algorithms for computing the TOPMODEL topographic index. *Water Resources Research*, 40 (W06303), 1–11. doi:10.1029/2004WR003069.

Qin, C.Z., *et al*., 2007. An adaptive approach to selecting a flow-partition exponent for a multiple-flow-direction algorithm. *International Journal of Geographical Information Science*, 21, 443–458.

Qin, C.Z., *et al*., 2009. Quantification of spatial gradation of slope positions. *Geomorphology*, 110, 152–161.

Qin, C.Z., *et al*., 2011. An approach to computing topographic wetness index based on maximum downslope gradient. *Precision Agriculture*, 12, 32–43.

Quinn, P., Beven, K.J., and Lamb, R., 1995. The $\ln(\alpha/\tan\beta)$ index: how to calculate it and how to use it within the TOPMODEL framework. *Hydrological Processes*, 9, 161–182.

Quinn, P., *et al*., 1991. The prediction of hillslope flow paths for distributed hydrological modeling using digital terrain models. *Hydrological Processes*, 5, 59–79.

Tarboton, D.G., 1997. A new method for the determination of flow directions and upslope areas in grid digital elevation models. *Water Resources Research*, 33, 309–319.

Wilson, J.P. and Gallant, J.C., eds., 2000. *Terrain Analysis: principles and applications*. New York (NY): John Wiley & Sons.

Wilson, J.P., *et al*., 2008. Water in the landscape: a review of contemporary flow routing algorithms. *In*: Q. Zhou, B. Lees, and G. Tang, eds. *Lecture notes in geoinformation and cartography: advances in digital terrain analysis*. Berlin: Springer, 213–236.

Wolock, D.M. and McCabe, G.J., 1995. Comparison of single and multiple flow direction algorithms for computing topographic parameters. *Water Resources Research*, 31, 1315–1324.

Zhan, L.-J., Qin, C.-Z., and Zhu, A.-X., 2012. Which type of slope gradient should be used to determine flow-partition proportion in multiple-flow-direction algorithms – tangent or sine? *Hydrology and Earth System Sciences Discussions*, 9, 6409–6418.

Zhou, Q. and Liu, X., 2002. Error assessment of grid-based flow routing algorithms used in hydrological models. *International Journal of Geographical Information Science*, 16, 819–842.

Zhou, Q., Pilesjö, P., and Chen, Y., 2011. Estimating surface flow paths on a digital elevation model using a triangular facet network. *Water Resources Research*, 47 (W07522), 1–12. doi:10.1029/2010WR009961.

Zhou, Q., *et al*., 2006. Terrain complexity and uncertainties in grid-based digital terrain analysis. *International Journal of Geographical Information Science*, 20, 1137–1147.